Computer-Assisted Determination of Orientation Relationships from Selected-Area Electron Diffraction: A Beginner's Guide to Pattern Indexing with RAPID-JS

Thomas E. Weirich †

Gemeinschaftslabor für Elektronenmikroskopie (GFE), RWTH Aachen University,
Ahornstr. 55, D-52074 Aachen

August 2026

Abstract Selected-area electron diffraction (SAED) in the transmission electron microscope (TEM) is a standard technique for determining crystallographic orientations and orientation relationships between different crystalline phases. This technical report presents a step-by-step approach for the computer-assisted indexing of SAED patterns from materials with cubic crystal symmetry using the web-browser based RAPID-JS program. The complete indexing workflow from the beginning until derivation of the orientation relationships is demonstrated using SAED patterns from an Fe–Si A2-type base alloy containing cube-on-cube, coherently oriented $D0_3$ precipitates.

1. Indexing of SAED patterns of materials with cubic crystal symmetry

The identification of orientation relationships is crucial for understanding precipitation hardening in metallic materials and is an established standard procedure in the crystallographic characterization of materials using selected-area electron diffraction (SAED) in the transmission electron microscope. As an example, Figure 1 shows two typical selected-area electron diffraction (SAED) spot patterns recorded from an A2 structure type [#] iron–silicon alloy containing coherently oriented $D0_3$ type precipitates. These diffraction patterns from cubic lattices display the characteristic cross-grating arrangement of diffraction spots, resulting from the superposition from the matrix (strong spots) and from the secondary phase (weak spots). Several manual approaches have been developed for indexing such SAED spot patterns from cubic lattices, and a variety of computer programs have been developed over the years to assist this task (see references in Weirich, 2024c, and Maroufidis & Weirich, 2025).

In the present technical report, the web-based application RAPID-JS (Weirich & Weirich, 2026) is employed for this purpose, as it can be used on all major computer systems with a standard web browser and is easy to learn, even for beginners.

† weirich@gfe.rwth-aachen.de

[#] https://aflowlib.org/prototype-encyclopedia

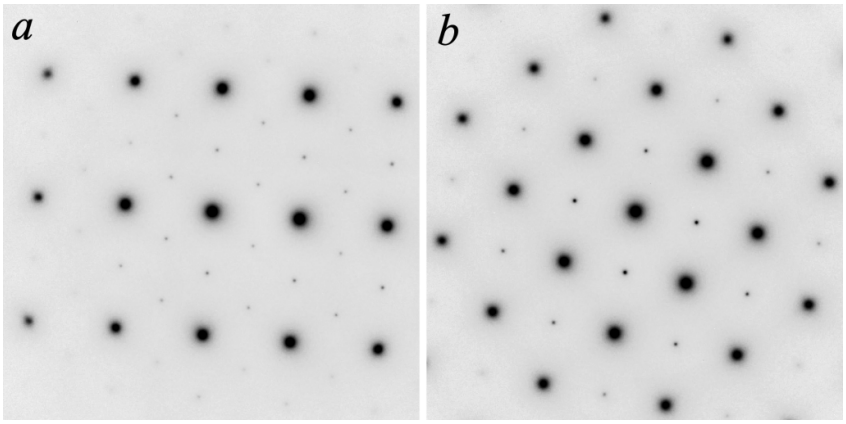


Figure 1. In a study on twin roll casting and secondary cooling of 6.0 wt.-% silicon steel (Müller *et al.*, 2021), the above-shown SAED cross-grating patterns were obtained at the present authors' TEM laboratory. Note that the primary beam in the pattern center has lost much of its intensity due to the strong scattering of the beam electrons and cannot be distinguished from the other diffraction spots. However, the geometry of the strong diffraction spots in both SAED patterns agree with the lattice of BCC ferrite or disordered $Fe_{0.67}Si_{0.33}$ (A2-structure type; Im3m space group symmetry). While the weak diffraction spots in (a) provide clear evidence for the presence of oriented $D0_3$ type precipitates (Fm3m space group symmetry), the weak diffraction spots observed in (b) allow no distinction between ordered B2-type (Pm-3m) and $D0_3$-type precipitates.

2. Lens-less electron diffraction geometry after G.P. Thomson

The geometry of lens-less electron diffraction is shown in Figure 2. Herein is r_{hkl} the distance of a diffraction spot from the pattern origin on the flat-panel detector and L is the distance of the diffracting crystal from the detector in real space. The corresponding parameters in reciprocal space are the distance $g_{hkl} = {d_{hkl}}^{-1}$ of a reciprocal lattice point from the origin, and λ^{-1} the radius of the Ewald sphere. If the electron wavelength is small for fast electrons, the (Bragg) diffraction angles θ are small too and the Ewald sphere can be approximated by a plane. This yields two right-angled triangles with the same gradient angle 2θ. Due to the geometrical similarity (*Strahlensatz*) of the two triangles, one can write:

$$ {r_{hkl}}/{L} = {g_{hkl}}/{\lambda^{-1}} = {{d_{hkl}}^{-1}}/{\lambda^{-1}} \quad \text{or} \quad r_{hkl} \cdot d_{hkl} = L \cdot \lambda = CC \tag{1} $$

Here, the product of the *de Broglie* wavelength of the electrons λ and the distance between the diffracting crystal and the detector plane L (*in the TEM, this distance is not real* [*]) is named the camera constant CC. The unit of the camera constant is determined by the unit of the measurement of the distance of the diffraction spot distance from the pattern center r_{hkl}. When evaluating a digital image, where distances between two points are usually measured in pixels, the unit of CC is Å·pixel. Note that the camera constant represents the magnification factor of the reciprocal lattice in the electron diffraction pattern as it is the ratio ${r_{hkl}}/{g_{hkl}}$ or ${r_{hkl}}/{{d_{hkl}}^{-1}}$ as shown in

[*] For electron diffraction in a TEM, the camera length L is just a virtual quantity, since the true diffraction pattern is formed in the back focal plane of the objective lens. From there it is enlarged by the microscope's projective system. The magnification factor CC_{OL} of the objective lens with the focal length f_{OL} (= L) for the reciprocal lattice is therefore $CC_{OL} = \lambda \cdot f_{OL}$. For the overall system of objective and projective lenses, the magnification factor is $CC_{TEM} = M_P \cdot CC_{OL}$, where M_P is the magnification factor of the projective system of the TEM.

Figure 2. The value of the camera constant is usually determined by measuring the ring radii in Debye-Scherrer-type electron diffraction patterns of nanocrystalline materials such as gold or thallium chloride and then multiplying the measured ring radii with the corresponding known d_{hkl} values (equation 1). The d_{hkl} values calculated with these camera constants are usually accurate enough to identify a phase from d_{hkl} lists of known structures. Thus, corrections for the camera constant, which have been occasionally suggested to improve accuracy (Lodder & v.d. Berg, 1974), can normally omitted in practical work. However, a detailed discussion of possible errors and their effect on the accuracy of the thereby determined d_{hkl} values can be found in Walck (Walck, 2020).

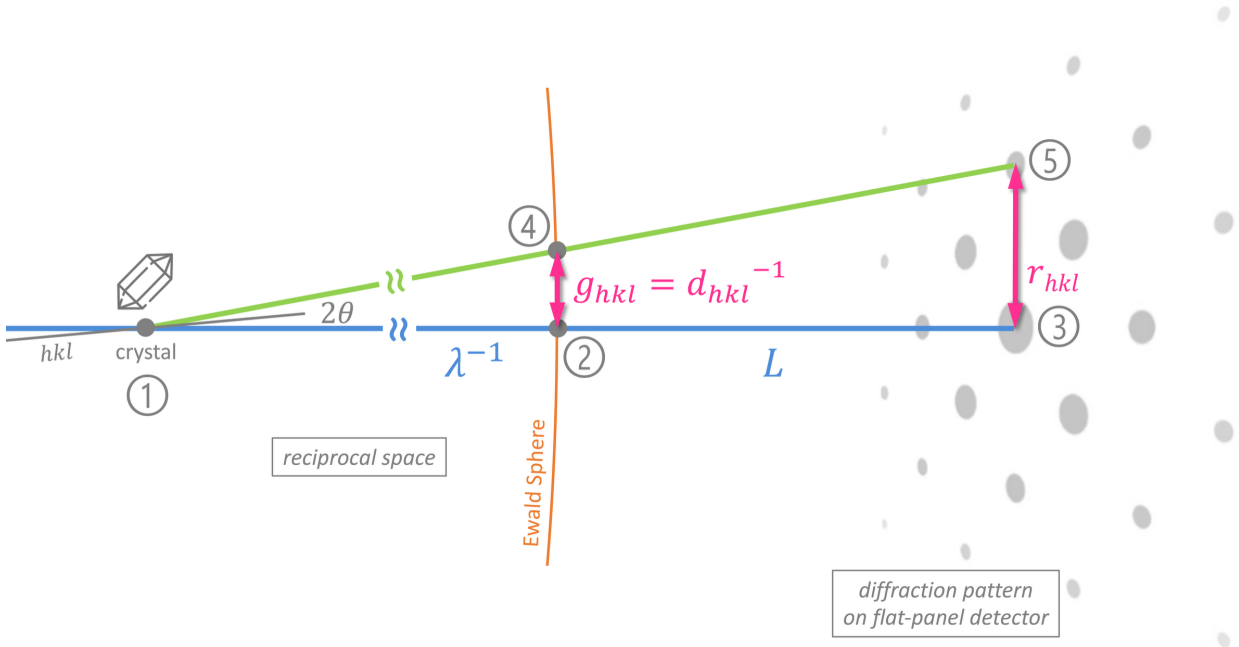


Figure 2. Geometry of lens-less diffraction of fast electrons after G. P. Thomson (Thomson & Cochrane, 1939). ① A crystal containing the lattice plane *hkl* is located at the center of the Ewald sphere, which has a radius of λ^{-1}, where λ is the electron wavelength. ② The origin of reciprocal space corresponds to the point where the non-diffracted (primary) electron beam exits the Ewald sphere. ③ Position of the primary beam on the flat-panel detector. The distance between the crystal at position ① and the primary beam at ③ is called the camera length, L, in real space. ④ A reciprocal-lattice point corresponding to the lattice plane *hkl* which is on, or very close to, the surface of the Ewald sphere. The vector connecting the reciprocal-lattice origin at ② and the reciprocal-lattice point is named g_{hkl}. For fast electrons, the curvature of the Ewald sphere is very small and can generally be neglected. Thus, the magnitude of the reciprocal-lattice vector becomes $g_{hkl} = d_{hkl}^{-1}$, where d_{hkl} is the interplanar spacing of the corresponding lattice planes in real space. The electron beam diffracted by the lattice plane *hkl* forms a diffraction spot at position ⑤ on the detector. The triangles defined by L and r_{hkl} in real space and λ^{-1} and d_{hkl}^{-1} in reciprocal space have the same included angle, 2θ, and are therefore geometrically similar (by the intercept theorem, *Strahlensatz*). Note that the ratio r_{hkl}/d_{hkl}^{-1} defines the magnification factor of the reciprocal lattice in the recorded diffraction pattern. This magnification factor is named the camera constant *CC* in electron diffraction.

Thomson, G. P., & Cochrane, W. (1939). Theory and practice of electron diffraction. Macmillan and Co.

3. The R_n Ratio Method for indexing cubic lattices

As shown by equation 1, the real space interplanar spacing d_{hkl} can be calculated from the distance r_{hkl} of a diffraction spot from the pattern center, if the magnification factor (the camera constant, *CC*) of the corresponding reciprocal lattice vector g_{hkl}, is known.

$$r_{hkl} = CC \cdot g_{hkl} = CC \cdot {}^{1}/_{d_{hkl}} \quad \Rightarrow \quad d_{hkl} = CC \cdot {}^{1}/_{r_{hkl}} \tag{2}$$

For crystals with a cubic lattice, the ratio of the lattice parameter a divided by the interplanar spacing d_{hkl} can be expressed by the Euclidian norm of the hkl indices. Replacement of d_{hkl} by relation (2) yields equations (3) and (4), respectively.

$$\sqrt{h^2 + k^2 + l^2} = {}^{a}/_{d_{hkl}} = r_{hkl} \cdot {}^{a}/_{CC} \qquad \left({}^{a}/_{CC} = const.\right) \tag{3}$$

$$\sqrt{h^2 + k^2 + l^2} \propto r_{hkl} \tag{4}$$

From the latter it can be derived that the ratio R_{12} of the distances of any two spots r_1 and r_2 from the pattern center is equal to the ratio of the Euclidian norms of their Laue indices hkl.

$$R_{12} = {}^{r_1}/_{r_2} = \sqrt{{h_1}^2 + {k_1}^2 + {l_1}^2} \Big/ \sqrt{{h_2}^2 + {k_2}^2 + {l_2}^2} \tag{5}$$

Thus (5) forms the basis of the *Rn*-ratio method. As (5) does not contain any information about the dimensions of the cubic lattice nor the magnification factor CC, it can also be applied on uncalibrated patterns. Note that this feature is unique and is generally valid only for the cubic lattice. As described in detail in the protocol for determining the zone axis direction from aligned SAED patterns of cubic materials (Weirich, 2024b), the practical work with the *Rn* ratio method involves the following manual steps:

1. Identifying the three pairs of symmetry related reflections A, B, and C that are closest to the pattern center, whereas A refers to the pair of diffraction spots with the shortest distance, B to the diffraction spots with the second shortest, and C to the pair of reflections with third-shortest distance (see Figure 3).

2. Measuring the distances between the reflections for each pair and divide the determined distances by two to obtain the distances r_A, r_B, and r_C of the diffraction spots from the pattern center. This approach of measuring the magnified reciprocal lattice vector lengths has been proven to be reliable and it avoids identifying the position of the center of the diffraction pattern first. The drawback of this method is however, that it is only applicable on near zone axis oriented SAED patterns, since it needs presence of three pairs of symmetry related reflections hkl and $\overline{hkl}$.

3. Measure the angles between the reflection pairs $\measuredangle AB$ and $\measuredangle AC$.

4. Calculate the ratios r_{BA} and r_{CA} and compare these values and the measured angles $\measuredangle AB$ and $\measuredangle AC$ with tabulated values for cubic crystals (Weirich, 2024a, Weirich, 2024b).

5. A found match for the experimental ratios and angles provides the corresponding hkl indices of the Laue diffraction spots and allows to determine the zone axis direction uvw for a standard setting (Weirich, 2024a, Weirich, 2024b).

All steps except the first step, the identifying the three pairs of symmetry related reflections, are supported by the RAPID-JS program (Weirich & Weirich, 2026), which enables users to instantly index SAED cross-grating patterns from cubic materials. However, as mentioned earlier, the evaluation procedure relies on three pairs of diffraction spots belonging to the same zone. Therefore, the program can only index SAED patterns from crystals that are closely oriented along a zone axis, like the pattern shown in Figure 1.

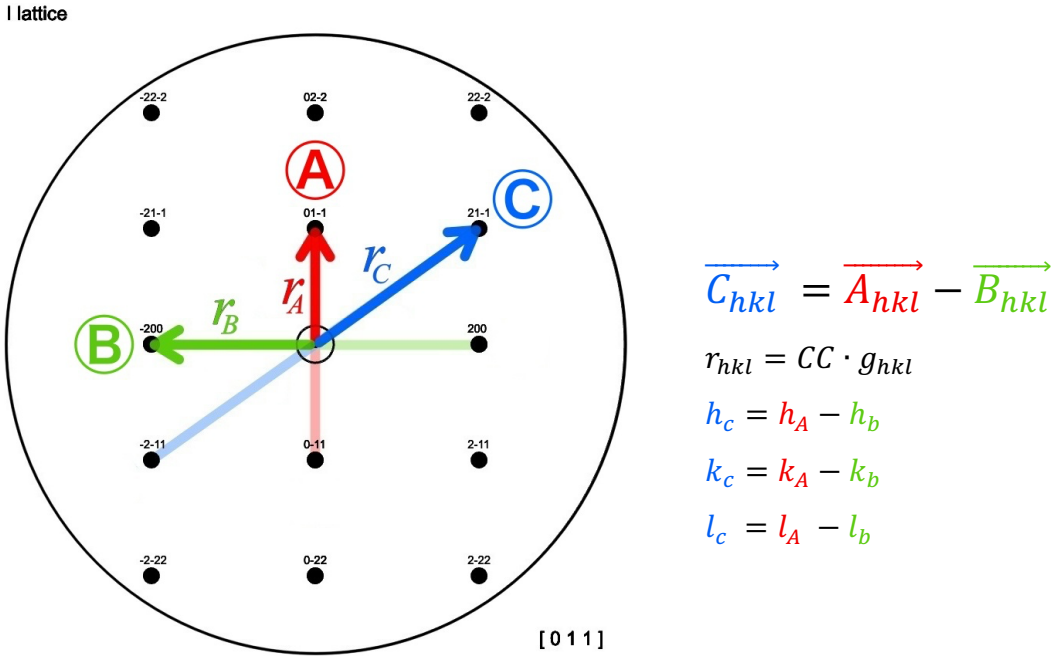


Figure 3. Calculated cross-grating spot pattern for the A2 structure type (space group Im3m) when the incident electron beam passes the specimen along the [011] direction. The ratio method for indexing a cross-grating spot pattern requires the three reflections A, B, and C to be measured. Note that A, B, C follow the order of increasing spot distances from the center of the diffraction pattern. In terms of representation as vectors, C is obtained by subtracting vector B from vector A, *i.e.* C(2 1 -1) = A(0 1 -1) – B(-2 0 0). For improved accuracy and avoiding determining the pattern center first, the distances of the diffraction spots from the center are determined by measuring the distance between the symmetry related opposite diffraction spots hkl and $\overline{hkl}$ and dividing the determined value by two to obtain the magnified length of the reciprocal vector r_{hkl}. Moreover, the method requires to measure the angles between the lines AB and AC. In the simplest approach for pattern indexing the determined ratios r_B/r_A and r_C/r_A and angles are compared with tabulated values of standard patterns (*e.g.* Weirich, 2024a, Weirich, 2024b). However, for practical work software assisted indexing of cross-grating spot patterns of cubic lattices is much faster. For this the RAPID family of programs, which are based on the above outlined relationships, have been optimised for this particular application (Weirich, 2024c; Maroufidis & Weirich, 2025; Weirich & Weirich, 2026).

4. Teaching Electron Diffraction with RAPID-JS

The latest version of RAPID-JS (Weirich & Weirich, 2026) can be obtained from the Zenodo repository at https://doi.org/10.5281/zenodo.18032072.

RAPID-JS is a user-friendly and easy to learn software tool that can be used for teaching and practical training of phase identification with SAED patterns from cubic materials. The indexing procedure of RAPID-JS provides a direct and intuitive way to relate the geometry of the experimentally recorded SAED patterns with the underlying reciprocal lattice and its crystallographic orientation. By interactively positioning the diffraction vectors and comparing the measured ratios and angles with the calculated geometries of cubic lattices, students gain a practical understanding of the principles of SAED pattern indexing, rather than relying on fully automated identification of diffraction patterns that is highlighted by other programs. In addition, the ready-to-use program facilitates its use in lectures, laboratory courses, and hands-on crystallography exercises because the program can be launched directly from a HTML file using a standard web browser and does not require any installation. Its small file size and platform-independent implementation also allow RAPID-JS to be distributed easily to students for independent study and practice. The SAED patterns used in this report are available for teaching purposes via the Zenodo repository at https://doi.org/10.5281/zenodo.21980782. This allows students to reproduce the indexing procedures described in this report independently.

5. Pattern indexing with RAPID-JS

The following section provides a step-by-step guide to indexing the SAED in Figure 1 using RAPID-JS. The indexing procedure is first demonstrated for the partial diffraction pattern of the A2-type steel matrix, followed by analysis of the diffraction pattern of the cubic precipitates.

After launching the program in a web-browser, three separate regions appear on the screen. There are panels on the left and right, and an empty central region when no diffraction pattern has been loaded. The panel labelled 'Diffraction pattern' on the left contains the file loader. The 'Lines' panel allows lines to be added one after another, while the 'Parameters' and 'Measurement' panels allow the camera constant and errors for the measurement to be set, as well as displaying the current measurement results. The panel on the right labelled 'Results' is only used to show the indexing results (see Figure 2).

Once the RAPID-JS user interface shows up in the web browser, a diffraction pattern can be loaded from the computer’s hard drive by clicking the 'Load SAED pattern' button in the file loader panel. Most web browsers support only JPG and PNG image formats. Thus, the original diffraction pattern may need to be converted to one of these formats before it can be loaded. An exception is the Safari web browser on macOS, which also supports images in TIFF format.

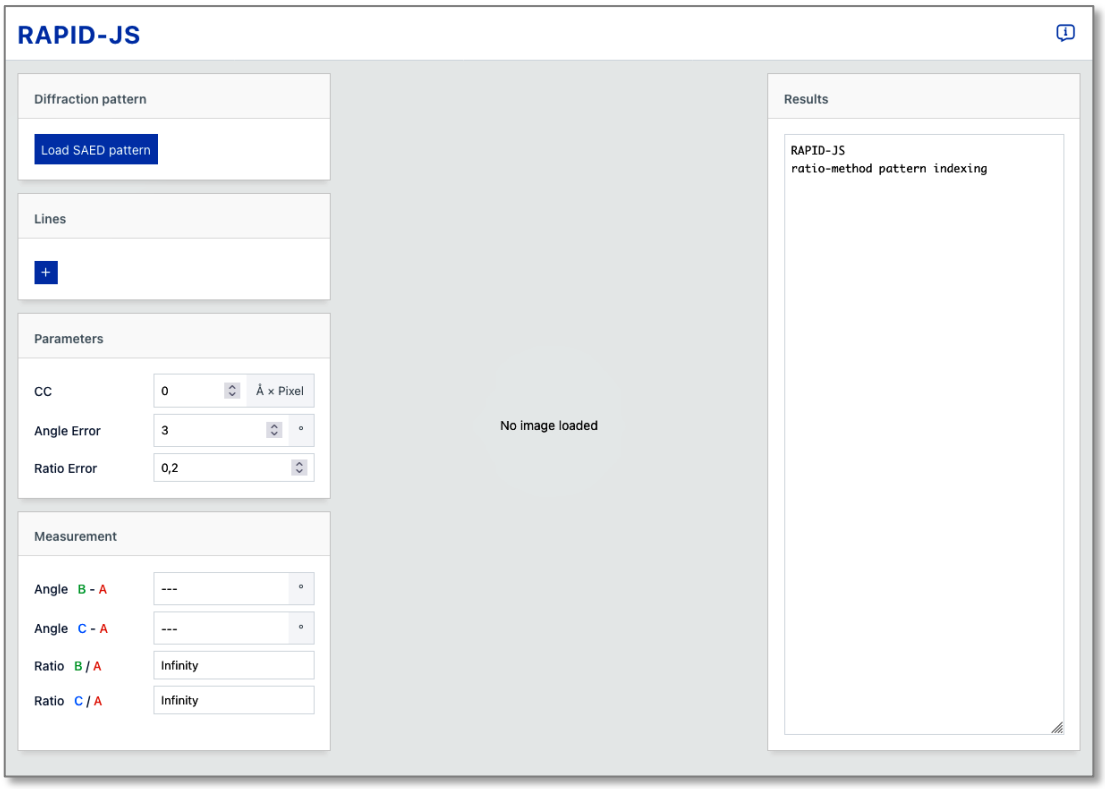


Figure 4. Appearance of RAPID-JS after launching the program in a web-browser. The panels on the left are the file loader and allow lines to be added, as well as to set the camera constant and errors for the measurement. The 'Measurement' (left side) and 'Results' (right side) panels are used by the program to show the measured angles, ratios and the indexing results, respectively.

If the camera constant CC is known, the value should be provided in the corresponding form field in the 'Parameters' panel. If CC is unknown or not available, the value should be set to zero, which is interpreted by RAPID-JS that the value of CC is unknown. If the user provides a value for the camera constant, the program will calculate an approximate lattice parameter from the measured diffraction spot distances. This is often helpful for identifying the correct solution if the program finds several matches for the pattern geometry.

In the 'Lines' panel on the left, the '+' button allows to add at maximum three line-tools for addressing the diffraction spots that are used for indexing. Each line-tool has a different color (red, green, and blue) and appears initially in the top-left region of the diffraction pattern. Each line has a filled circle at both ends, which are called *handles*. An orange handle on one side of each line remains visible at all times, whereas a second handle in the corresponding line color becomes visible only when the mouse pointer is moved close to a line. If the mouse pointer is positioned over a handle, the handle can be moved by pressing and holding the left mouse button. The orange handles of the lines, which are always visible, have a special function as they must be positioned on the diffraction spots that correspond to the vectors A, B, and C in Figure 3.

To index the diffraction pattern of the metallic matrix in Figure 1a, the orange handle of the red line is dragged onto one of the diffraction spots with strong intensity nearest to the center. The orange handle of the red line has also an additional special function, as it defines a reference point for indexing the diffraction pattern. This can be visualized using a clock analogy, where the orange handle of the red line represents the 12 o'clock position. Therefore, when defining the first (red) line, the user is free to choose which of the two diffraction spots closest to the pattern center should serve as this reference point. For the pattern shown in Figure 5a the diffraction spot marked with ① has been selected as reference. The positions of the orange handles of the two other lines (green and blue), however, must now follow some rules which are outlined in the following.

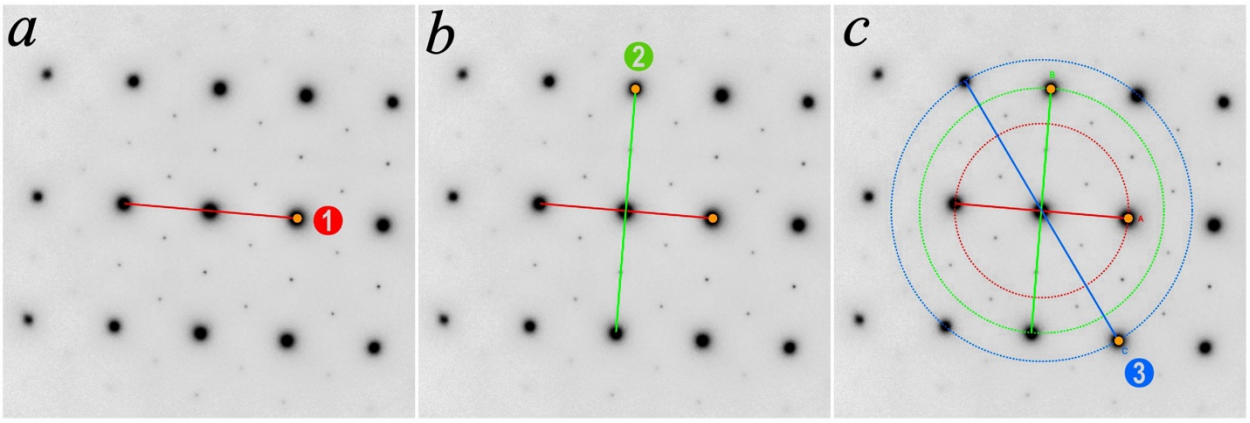


Figure 5. Sequence for assigning diffraction spots in the SAED pattern of Figure 1a for pattern indexing with RAPID-JS. As outlined in the main text, the three pairs of symmetry-related reflections closest to the pattern center are assigned in the order A, B, and C, following the number labels. The orange circle at the end of each coloured line represents the endpoint (pointer) of the corresponding vectors A, B, and C shown in Figure 3. First, the pair of reflections with the shortest distance from the pattern center is assigned by placing the orange handle of the red line at position ①, as shown in (a). Next, the orange handle of the green line is placed on the diffraction spot corresponding to the second-shortest distance, located to the *left* of position ①, *i.e.*, at position ②, as shown in (b). Finally, the orange handle of the blue line is positioned on the diffraction spot corresponding to the third-shortest distance, located to the *right* of position ①, *i.e.*, at position ③, as shown in (c). Once a common intersection point of the three lines is approached, circles are drawn around the intersection point of the three lines which simplifies the subsequent fine-tuning and adjustments of the endpoint positions of the lines on the diffraction spots.

After the red line has been positioned, the next (green) line is added via the '+' button. The handles of the green line must then be placed on the pair of second-closest diffraction spots. However, to obtain a correct solution, the orange handle of the green line must be positioned on the diffraction spot marked by ②, which is located to the *left* (counterclockwise direction) of the orange handle of the red line (see Figure 5b).

Finally, the blue line is added to connect the pair of third-closest diffraction spots. As illustrated in Figure 3, diffraction spot C, indicated by ③ in Figure 5c, is obtained by subtracting vector B from vector A. Consequently, the diffraction spot at the endpoint of the blue line must be located to the *right* (clockwise) of the orange handle of the red line. Once the three lines intersect at a common point, circles are displayed as a visual aid to facilitate the fine adjustment of the line endpoints on the diffraction spots. As soon as the user-defined pattern geometry matches the pre-calculated geometry of the ideal cubic lattice within the defined errors limits, the corresponding result is immediately displayed in the 'Results' panel on the right-hand side (see Figure 6). If the 'Results' panel displays too many possible solutions, the best-fitting match can quickly be identified by progressively reducing the angle and ratio error tolerances until only a few indexing solutions remain. For the present case of the SAED pattern in Figure 1, the two remaining solutions are shown in Table 1.

A brief note on the accuracy of the numerical results — The by RAPID-JS calculated lattice parameter is obtained as the mean value of the experimental interplanar spacings and should therefore be regarded as a rough estimate. The same applies to the calculated interplanar spacings, as the manual positioning of diffraction spots with the mouse pointer is inherently limited in accuracy and precision. Consequently, the level of precision displayed in Table 1 to three decimal places cannot be achieved by the here employed measurement method. These values should therefore be interpreted with some caution. Nevertheless, practical experience has shown that the estimated lattice parameter is often sufficient for database searches and for save distinguishing

between different indexing solutions. For the present example, the lattice parameters of Fe–Si alloys with space group Im3m listed in the current version of the ICDD PDF-5 database range from a = 2.810 Å (PDF entry 04-002-3903) to a = 2.873 Å (PDF entry 04-017-6672). The lattice parameter, determined from the SAED pattern in Figure 1a, is a = 2.854 Å and fits well within this range.

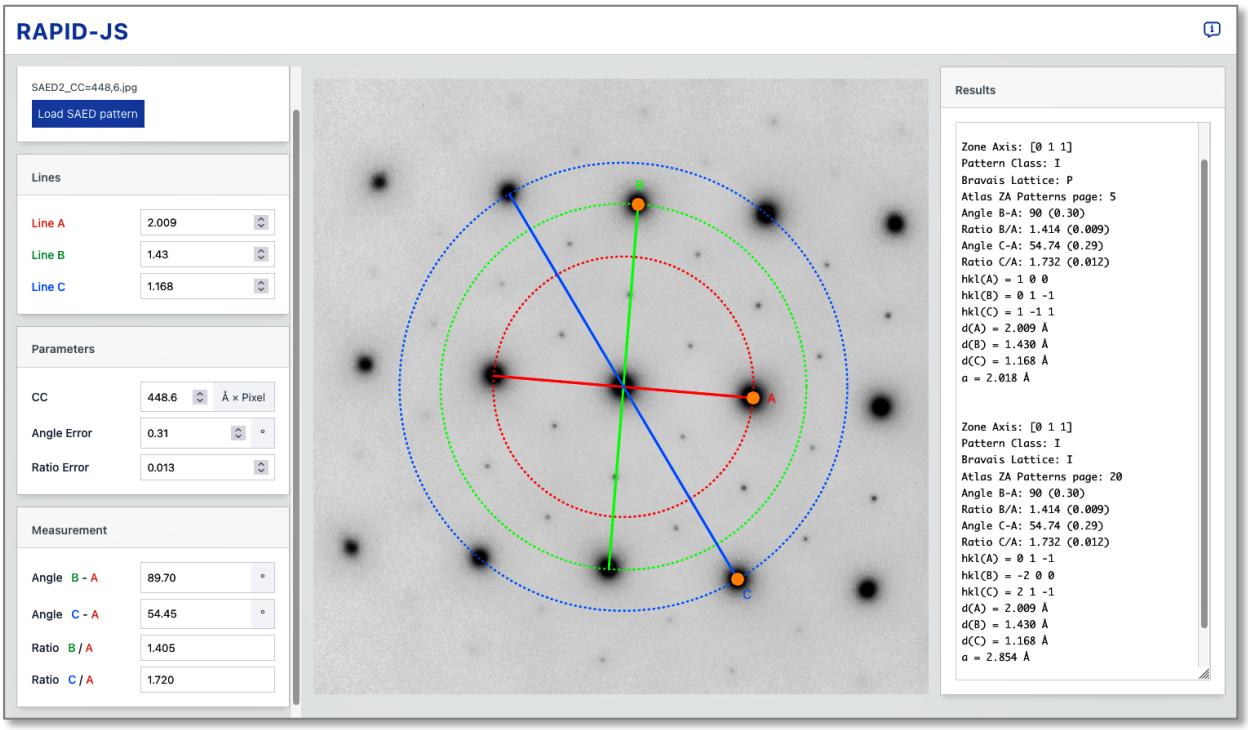


Figure 6. Appearance of RAPID-JS after processing the SAED pattern shown in Figure 1a / Figure 5. The indexing results that geometrically match the experimentally measured values displayed on the left in the 'Measurement' panel are listed in the 'Results' panel on the right. If the results list contains too many solutions because the default tolerances for the angle error and/or ratio error are too large, the following procedure is recommended to identify the best-fitting solutions. First, set the angle error in the 'Parameters' panel to zero to clear the 'Results' panel. Then increase the angle error in small increments using the up arrow in the corresponding input field until the first solution appears. Repeat the same procedure for the ratio error setting in the 'Parameters' panel. To access the results list, click on the right-hand panel with the mouse pointer, then 'select all' with the right mouse button, and copy the list for later import into another program. To export the processed diffraction pattern with the overlays, right-click on the image and use the image export function provided by the web browser.

The processing of the other diffraction pattern in Figure 1b is essentially identical to the procedure described above. However, this pattern represents a special case, as it contains four diffraction spots ideally located at the same distance from the pattern center. Thus, the straightforward strategy of sequentially addressing pairs of symmetry-related diffraction spots with increasing distances from the pattern center cannot be used here. Besides for the [001] zone-axis patterns of primitive (P), body-centered (I), and face-centered (F) cubic lattices, this characteristic is found in the [011] zone-axis pattern of face-centered (F) cubic lattices (Weirich, 2024b). However, the principle of the arrangement of the three vectors remains the same for this pattern. Thus, the diffraction spots marked by the orange handles of the red and green lines must be selected such that the orange handle of the green line ② in Figure 7b is positioned to the *left* (counterclockwise) of the orange handle of the red line ① in Figure 7a. Again, the position of the orange handle of the blue line ③ is obtained by subtracting vector B from vector A, which yields the position of diffraction spot ③ (see Figure 7c).

Zone Axis: [0 1 1]	**Zone Axis: [0 1 1]**
Pattern Class: I	**Pattern Class: I**
Bravais Lattice: P	**Bravais Lattice: I**
Atlas ZA Patterns page: 5	**Atlas ZA Patterns page: 20**
Angle B-A: 90 (0.30)	**Angle B-A: 90 (0.30)**
Ratio B/A: 1.414 (0.009)	**Ratio B/A: 1.414 (0.009)**
Angle C-A: 54.74 (0.29)	**Angle C-A: 54.74 (0.29)**
Ratio C/A: 1.732 (0.012)	**Ratio C/A: 1.732 (0.012)**
hkl(A) = 1 0 0	**hkl(A) = 0 1 -1**
hkl(B) = 0 1 -1	**hkl(B) = -2 0 0**
hkl(C) = 1 -1 1	**hkl(C) = 2 1 -1**
d(A) = 2.009 Å	**d(A) = 2.009 Å**
d(B) = 1.430 Å	**d(B) = 1.430 Å**
d(C) = 1.168 Å	**d(C) = 1.168 Å**
a = 2.018 Å	**a = 2.854 Å**

Table 1. The two indexing solutions obtained after processing the SAED pattern in Figure 1a / Figure 5 with RAPID-JS. For each solution, the results include the standard zone-axis orientation [*uvw*], the Bravais lattice type, the measured deviations (errors) from the ideal interplanar spacing ratios and interplanar angles (deviation in parentheses), and the *hkl* Laue indices of the three reflections A, B, and C. In addition, the pattern class (see Weirich, 2024b) and the corresponding page number in the *Atlas of Zone Axis Patterns of Cubic Lattices* (Weirich, 2024a) are provided for reference. Because the camera constant has been defined in this example, the interplanar spacings d_{hkl} for the indexed reflections and an estimated lattice parameter a are calculated for each solution. In the present case, this makes it possible to reject the first solution (P lattice, a = 2.018 Å), whereas the second solution (I lattice, a = 2.854 Å) is consistent with the expected lattice parameter of the BCC metallic matrix.

Zone Axis: [0 0 1]	**Zone Axis: [0 0 1]**	Zone Axis: [0 0 1]	Zone Axis: [0 0 1]
Pattern Class: I	**Pattern Class: I**	Pattern Class: I	Pattern Class: I
Bravais Lattice: P	**Bravais Lattice: I**	Bravais Lattice: F	Bravais Lattice: D
Atlas ZA Patterns page: 4	**Atlas ZA Patterns page: 19**	Atlas ZA Patterns page: 34	Atlas ZA Patterns page: 49
Angle B-A: 90 (0.23)	**Angle B-A: 90 (0.23)**	Angle B-A: 90 (0.23)	Angle B-A: 90 (0.23)
Ratio B/A: 1 (0.015)	**Ratio B/A: 1 (0.015)**	Ratio B/A: 1 (0.015)	Ratio B/A: 1 (0.015)
Angle C-A: 45 (0.14)	**Angle C-A: 45 (0.14)**	Angle C-A: 45 (0.14)	Angle C-A: 45 (0.14)
Ratio C/A: 1.414 (0.012)	**Ratio C/A: 1.414 (0.012)**	Ratio C/A: 1.414 (0.012)	Ratio C/A: 1.414 (0.012)
hkl(A) = 1 0 0	**hkl(A) = 1 1 0**	hkl(A) = 2 0 0	hkl(A) = 2 2 0
hkl(B) = 0 1 0	**hkl(B) = -1 1 0**	hkl(B) = 0 2 0	hkl(B) = -2 2 0
hkl(C) = 1 -1 0	**hkl(C) = 2 0 0**	hkl(C) = 2 -2 0	hkl(C) = 4 0 0
d(A) = 2.036 Å	**d(A) = 2.036 Å**	d(A) = 2.036 Å	d(A) = 2.036 Å
d(B) = 2.005 Å	**d(B) = 2.005 Å**	d(B) = 2.005 Å	d(B) = 2.005 Å
d(C) = 1.428 Å	**d(C) = 1.428 Å**	d(C) = 1.428 Å	d(C) = 1.428 Å
a = 2.020 Å	**a = 2.857 Å**	a = 4.040 Å	a = 5.714 Å

Table 2. Possible solutions after processing the SAED pattern in Figure 7 with RAPID-JS. Again, all solutions except the second (I lattice, a = 2.857 Å) can be rejected, as it is the only solution consistent with the expected lattice parameter of the BCC metallic matrix.

The four indexing solutions for the pattern in Figure 7 are shown in Table 2. Since the pattern geometry alone does not allow to distinguish between the P, I, F, and D (diamond) lattice types, this example demonstrates the great value of having a camera constant for the processed pattern. Thus, all solutions except the second can be ruled out using the lattice-parameter criterion. It is noteworthy that the determined lattice parameter was reproduced with remarkable accuracy (2.854 Å vs. 2.857 Å), despite the two SAED patterns were recorded from different grains and orientations and the diffraction spot positions were only roughly addressed by mouse pointer.

Indexing the weak diffraction spots of the partial patterns from the coherently oriented $D0_3$-type precipitates in the SAED patterns follows the above outlined principles. Figures 8 and 9 show enlarged views of the central regions of the respective patterns around the primary electron beam. Note that the partial patterns of weak diffraction spots in Figures 8 and 9 both belong to the class of patterns characterized by four diffraction spots at equal distances from the primary beam. Hence, the processing is analogous as described for the pattern in Figure 7. The corresponding indexing results are listed in Tables 3 and 4.

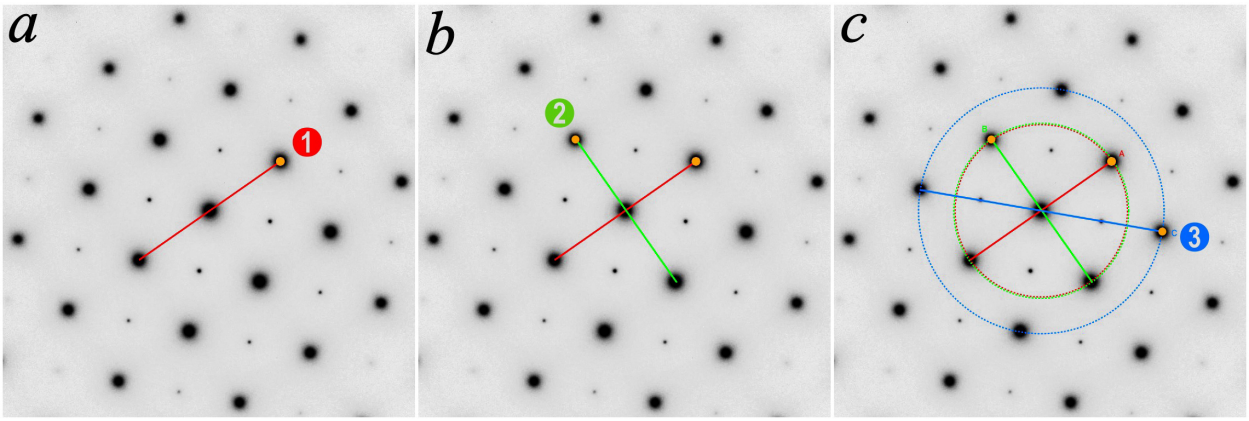


Figure 7. Sequence for assigning the A2 matrix diffraction spots in the SAED pattern of Figure 1b. Due to the 4-fold pattern symmetry, two pairs of reflections at the same (shortest) distance are present. Therefore, the orange handle of the red line must be positioned on one pair of diffraction spots so that the orange handle of the green line is placed to the *left*. This is shown in (a) and (b). Finally, the orange handle of the blue line must be positioned, as before, on diffraction spot A–B at ③, to the *right* of the orange handle of the red line, as shown in (c).

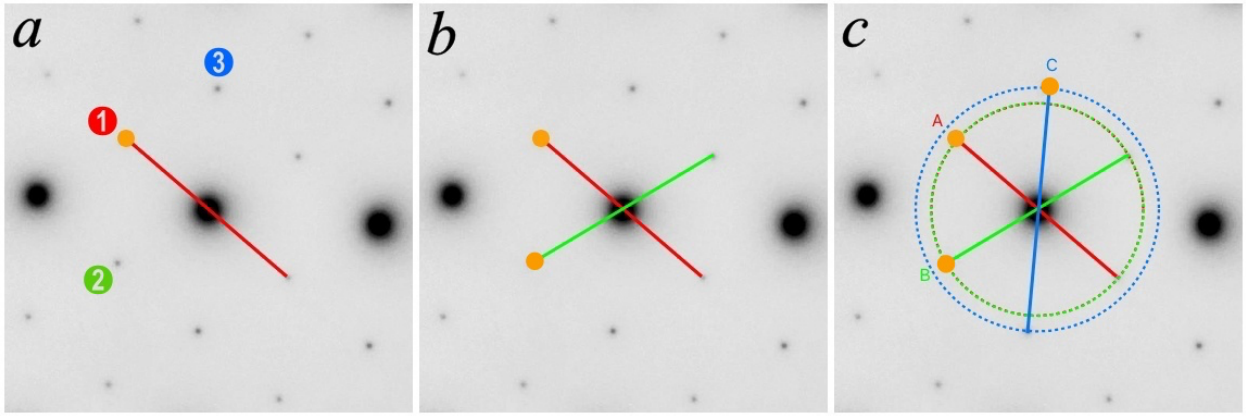


Figure 8. The centre region of the SAED pattern of Figure 1a / Figure 5 shows the weak diffraction spots of the oriented $D0_3$-type precipitates. The pattern formed by the weak diffraction spots has four diffraction spots with equal distances from the centre. Thus, the red and green lines must be drawn as shown in (b), with the orange handle of the green line *left* of the orange handle of the red line. The postion of the orange handle of the blue line is assigned regularly as shown in (c) and obtained by subtracting vector B from vector A.

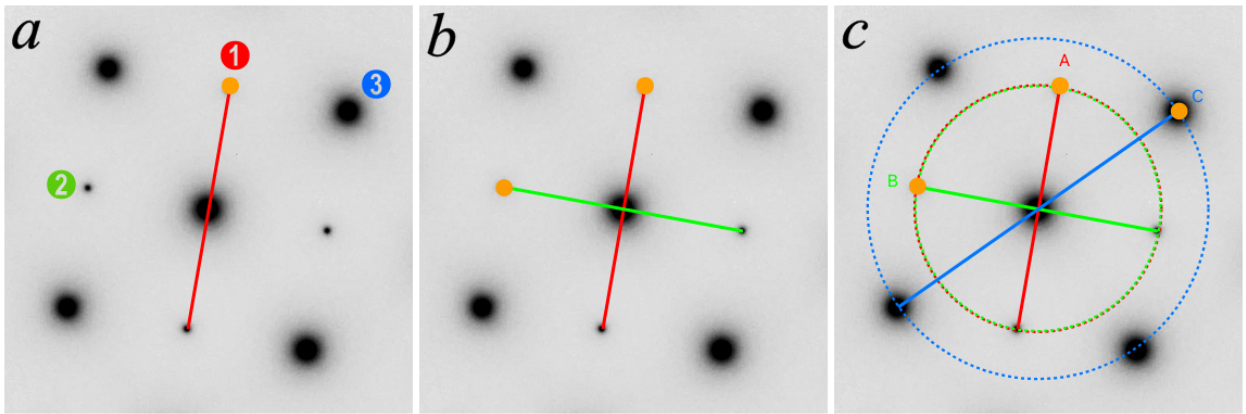


Figure 9. The centre region of the SAED pattern of Figure 1b / Figure 7 shows the weak diffraction spots of the oriented $D0_3$-type precipitates. The rules for indexing the pattern formed by the weak diffraction spots is the same as for Figure 7. Note that the observed pattern geometry and intensity distribution is also typical of primitive cubic structures, such as ABO_3 perovskites, or in this case, the ordered iron-silicon α' phase (B2 structure type). Therefore, the geometry of this diffraction pattern alone cannot distinguish between the B2 and $D0_3$-structure type (see Figures 12b and 12c).

Zone Axis: [0 1 1]	Zone Axis: [0 1 1]
Pattern Class: III	Pattern Class: III
Bravais Lattice: F	Bravais Lattice: D
Atlas ZA Patterns page: 35	Atlas ZA Patterns page: 50
Angle B-A: 70.53 (1.12)	Angle B-A: 70.53 (1.12)
Ratio B/A: 1 (0.003)	Ratio B/A: 1 (0.003)
Angle C-A: 54.74 (1.27)	Angle C-A: 54.74 (1.27)
Ratio C/A: 1.155 (0.007)	Ratio C/A: 1.155 (0.007)
hkl(A) = 1 1 -1	hkl(A) = 1 1 -1
hkl(B) = -1 1 -1	hkl(B) = -1 1 -1
hkl(C) = 2 0 0	hkl(C) = 2 0 0
d(A) = 3.284 Å	d(A) = 3.284 Å
d(B) = 3.275 Å	d(B) = 3.275 Å
d(C) = 2.860 Å	d(C) = 2.860 Å
a = 5.694 Å	a = 5.694 Å

Table 3. Possible indexing solutions obtained after processing the weak diffraction spots in the SAED pattern in Figure 8 with RAPID-JS. The pattern of the identified [011] orientation is compatible with the standard F-centered cubic lattice, or the F-centered lattice with diamond glide plane (D). For deciding between the two solutions, an ICDD database search with lattice parameter a = 5.694 Å ± 0.1 Å and iron and silicon was performed, which yielded only entries for $D0_3$-type Fe_3Si with space group Fm3m. Therefore, the diamond-structured solution could be ruled out. The corresponding fully indexed pattern is shown in Figure 11b.

Zone Axis: [0 0 1]	Zone Axis: [0 0 1]	**Zone Axis: [0 0 1]**	Zone Axis: [0 0 1]
Pattern Class: I	Pattern Class: I	**Pattern Class: I**	Pattern Class: I
Bravais Lattice: P	Bravais Lattice: I	**Bravais Lattice: F**	Bravais Lattice: D
Atlas ZA Patterns page: 4	Atlas ZA Patterns page: 19	**Atlas ZA Patterns page: 34**	Atlas ZA Patterns page: 49
Angle B-A: 90 (0.05)	Angle B-A: 90 (0.05)	**Angle B-A: 90 (0.05)**	Angle B-A: 90 (0.05)
Ratio B/A: 1 (0.007)	Ratio B/A: 1 (0.007)	**Ratio B/A: 1 (0.007)**	Ratio B/A: 1 (0.007)
Angle C-A: 45 (0.41)	Angle C-A: 45 (0.41)	**Angle C-A: 45 (0.41)**	Angle C-A: 45 (0.41)
Ratio C/A: 1.414 (0.034)	Ratio C/A: 1.414 (0.034)	**Ratio C/A: 1.414 (0.034)**	Ratio C/A: 1.414 (0.034)
hkl(A) = 1 0 0	hkl(A) = 1 1 0	**hkl(A) = 2 0 0**	hkl(A) = 2 2 0
hkl(B) = 0 1 0	hkl(B) = -1 1 0	**hkl(B) = 0 2 0**	hkl(B) = -2 2 0
hkl(C) = 1 -1 0	hkl(C) = 2 0 0	**hkl(C) = 2 -2 0**	hkl(C) = 4 0 0
d(A) = 2.816 Å	d(A) = 2.816 Å	**d(A) = 2.816 Å**	d(A) = 2.816 Å
d(B) = 2.837 Å	d(B) = 2.837 Å	**d(B) = 2.837 Å**	d(B) = 2.837 Å
d(C) = 2.041 Å	d(C) = 2.041 Å	**d(C) = 2.041 Å**	d(C) = 2.041 Å
a = 2.846 Å	a = 4.026 Å	**a = 5.693 Å**	a = 8.051 Å

Table 4. The table shows the possible indexing solutions obtained after processing the weak diffraction spots in the SAED pattern shown in Figure 9. Due to the apparent geometrical similarity of the full patterns in Figures 12b and 12c, it is not possible to discriminate between iron-silicon B2-type α' precipitates (space group symmetry Pm-3m) and $D0_3$-type α'' precipitates (space group symmetry Fm3m). However, as the diffraction pattern was taken from the same sample region and given that the other pattern of weak reflections in Figure 1a / Figure 11b is only compatible with $D0_3$-type precipitates, it could be argued that the full pattern indexed for the D03-type in Figure 12c is the most likely solution.

6. Derivation of the Crystallographic Orientation Relationship

The iron-silicon system investigated here is characterised by the development of congruent secondary phases that follow the sequence α (disordered A2-type) → α′ (B2-type) → α′′ ($D0_3$-type), with increasing cation ordering. Thus, the strong geometric relationships between the α (A2-type) metallic matrix and the secondary phases complicate the interpretation of the indexing results for certain crystal orientations, as some SAED patterns do not allow for an unambiguous distinction between the possible secondary phases. Figure 10 shows which of the common matrix orientations can be used to discriminate between A2 and B2 structures. To decide between the B2 and $D0_3$ structures, SAED patterns with orientations <011>, <134>, <123> and <112> can be used. The presence of the $D0_3$-type precipitates is always confirmed if the prominent {111} diffraction spots at approximately 3.28 Å of the F-lattice are detected alongside superstructure diffraction spots that also match also with the B2 structure. If the {111} diffraction spots are absent, the structure belongs to the B2-type.

As Figures 1a and 8 respectively clearly show the {111} diffraction spots, the indexing results obtained for the [011] orientation in Table 3 disprove the presence of a primitive B2-type lattice and are only consistent with either a standard face-centred cubic lattice or a face-centred lattice with a diamond glide plane (D). For deciding between the two possibilities, an ICDD database search with lattice parameter a = 5.694 Å ± 0.1 Å and iron and silicon was performed, which yielded only entries for $D0_3$-type Fe_3Si with space group Fm3m. Therefore, the diamond-structure could be ruled out. The corresponding fully indexed SAED pattern for the $D0_3$-type is shown in Figure 11b.

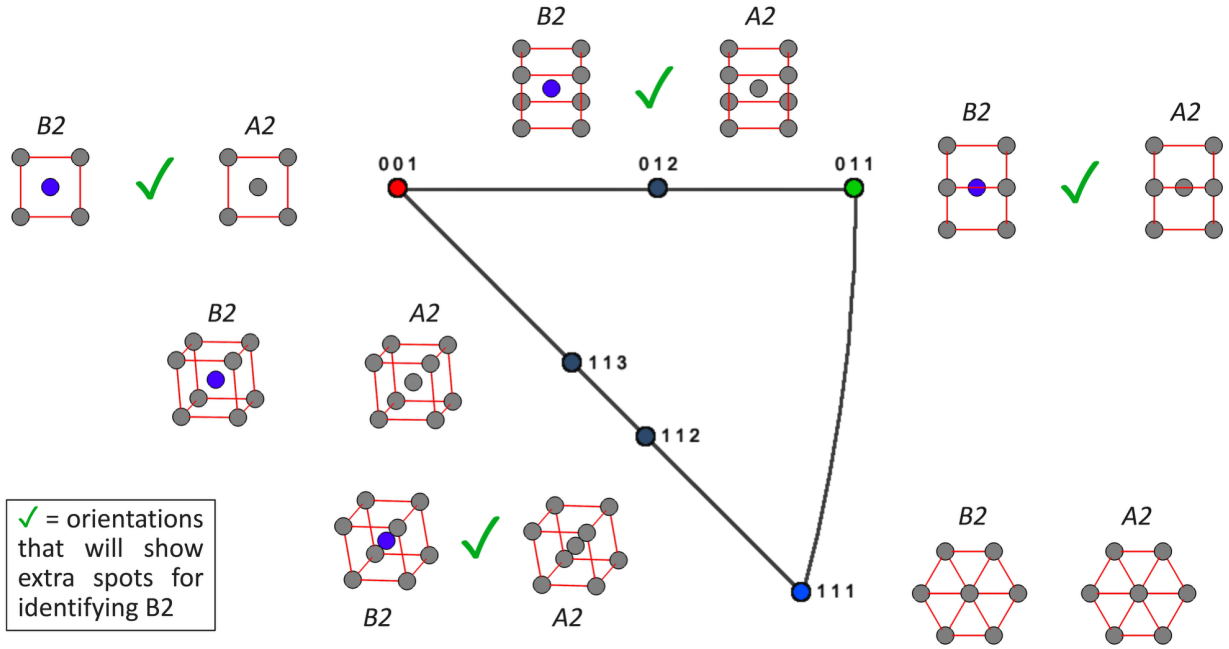


Figure 10. The figure shows which of the commonly encountered matrix orientations can be used to distinguish between the A2 and B2 structures. In addition, the orientations <011> and <112> can be used to further discriminate between B2 and $D0_3$-type precipitates (see main text).

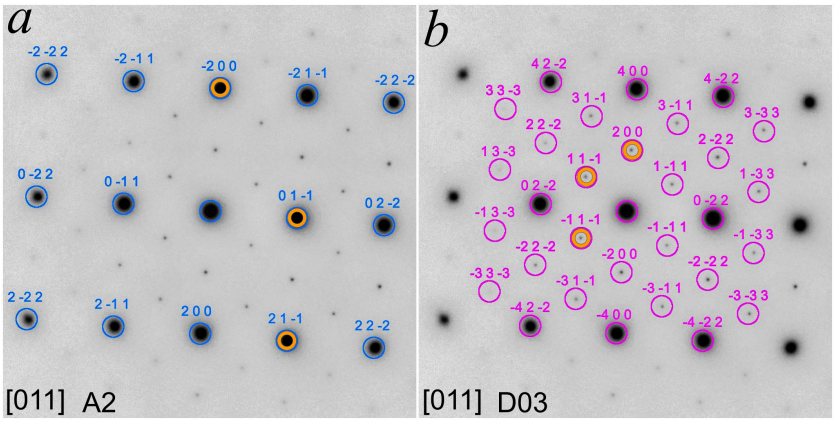


Figure 11. (a) Experimental SAED pattern from Figure 1a, with Laue indices for the A2-type base material corresponding to the second solution (I lattice, a = 2.854 Å) in Table 1. (b) Indexed SAED patterns of the weak diffraction spots observed in Figures 1a and 8, respectively, based on the first solution listed in Table 3 (F lattice, a = 5.694 Å). The latter is consistent with the $D0_3$-type structure of Fe_3Si. Diffraction spots marked by additional circles in orange refer to the reflections used for indexing with RAPID-JS (see Figures 5 and 8).

The SAED pattern in Figures 1b and 9, respectively, is not as straightforward to interpret as in the latter case. Due to the apparent geometrical similarity of the indexed patterns in Figures 12b and 12c, it is not possible to distinguish between iron-silicon B2-type α' precipitates (space group symmetry Pm3m) and $D0_3$-type α'' precipitates (space group symmetry Fm3m). However, as the diffraction pattern was taken from the same sample region and given that the other pattern of weak reflections in Figure 11b is only compatible with $D0_3$-type precipitates, it could be argued that the pattern for the $D0_3$-type in Figure 12c is again the most likely solution.

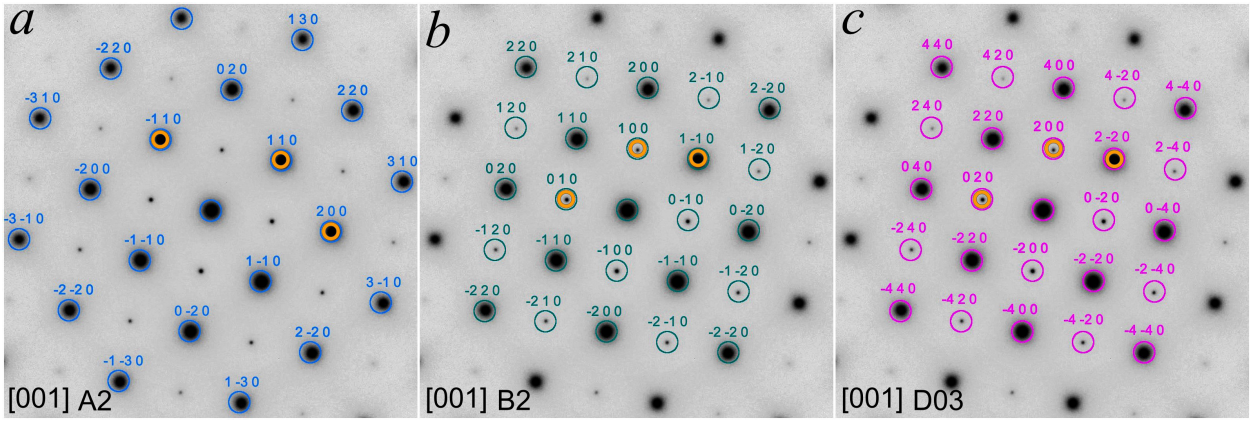


Figure 12. (a) Experimental SAED pattern from Figure 1b, with Laue indices for the A2-type matrix corresponding to the second solution in Table 2 (I lattice, a = 2.857 Å). The fully indexed SAED pattern for the B2-type (first solution in Table 4, P lattice, a = 2.846 Å) and for the $D0_3$-type (third solution in Table 4, F lattice, a = 5.693 Å) are shown in Figures 12b and 12c. The interpretation as $D0_3$-type in Figure 12c is ranked as the most likely solution (see main text).

Assuming that both SAED patterns represent a $D0_3$-type secondary phase oriented with the A2 metallic matrix, the following orientation relationships can be readily obtained from the indexed patterns. From Figure 11a and 11b the following orientation relationship is obtained:

$$[0\,1\,1]_{A2} \parallel [0\,1\,1]_{D03}$$
$$(-1\,0\,0)_{A2} \parallel (1\,0\,0)_{D03}$$

Note that in contrast to Laue indices in the indexed diffraction patterns, the Miller indices for crystal faces (!) are always coprime and are written in parentheses ( ). The Miller indices for A2 can easily be transformed into the following form using the comprehensive reindexing tables (Weirich, 2026). The latter yields the same Miller indices for both crystal species.

$$(1\,0\,0)_{A2} \parallel (1\,0\,0)_{D03}$$

Correspondingly, the following orientation relationship is obtained from Figures 12a and 12c after transforming the Miller indices:

$$[0\,0\,1]_{A2} \parallel [0\,0\,1]_{D03}$$
$$(0\,1\,0)_{A2} \parallel (1\,0\,0)_{D03} \rightarrow (1\,0\,0)_{A2} \parallel (1\,0\,0)_{D03}$$

Thus, evaluation of both SAED patterns returns the same orientation relationship which is known as *cube-on-cube* (Burke, 2016) and has the general form:

$$\langle 0\,0\,1 \rangle_{A2} \parallel \langle 0\,0\,1 \rangle_{D03}$$
$$\{1\,0\,0\}_{A2} \parallel \{1\,0\,0\}_{D03}$$

Acknowledgements The SAED patterns used in this report were recorded by Mr. Sebastian Zischke (GFE). The sample was kindly provided by Dr. Max Müller (Institute of Metal Forming, RWTH Aachen University). This work has been carried out within the Collaborative Research Centre Transregio 188: Damage Controlled Forming Processes (DFG – German Research Foundation, Project-ID 278868966).